

Multigrid-in-Channels Neural Network Architectures

Moshe Eliasof

Department of Computer Science
Ben-Gurion university of the Negev
eliasof@post.bgu.ac.il

Lars Ruthotto

Department of Mathematics
and Computer Science
Emory University
lruthotto@emory.edu

Jonathan Ephrath

Department of Computer Science
Ben-Gurion university of the Negev
ephrathj@post.bgu.ac.il

Eran Treister

Department of Computer Science
Ben-Gurion university of the Negev
erant@cs.bgu.ac.il

Abstract

We present a multigrid-in-channels (MGIC) approach that tackles the quadratic growth of the number of parameters with respect to the number of channels in standard convolutional neural networks (CNNs). It has been shown that there is a redundancy in standard CNNs, as networks with light or sparse convolution operators yield similar performance to full networks. However, the number of parameters in the former networks also scales quadratically in width, while in the latter case, the parameters typically have random sparsity patterns, hampering hardware efficiency. Our approach for building CNN architectures scales linearly with respect to the network’s width while retaining full coupling of the channels as in standard CNNs. To this end, we replace each convolution block with its MGIC block utilizing a hierarchy of lightweight convolutions. Our extensive experiments on image classification, segmentation, and point cloud classification show that applying this strategy to different architectures like ResNet and MobileNetV3 considerably reduces the number of parameters while obtaining similar or better accuracy. For example, we obtain 76.1% top-1 accuracy on ImageNet with a lightweight network with similar parameters and FLOPs to MobileNetV3.

1. Introduction

Convolutional neural networks (CNNs) [31] have achieved impressive accuracy for image classification, semantic segmentation, and many other imaging tasks [30, 14]. The main idea behind CNNs is to define the linear operators in the neural network as convolutions with local kernels. This increases the network’s computational efficiency (com-

pared to the original class of networks) due to the essentially sparse convolution operators and the considerable reduction in the number of weights. The general trend in the development of CNNs has been to make deeper, wider, and more complicated networks to achieve higher accuracy [44].

In practical applications of CNNs, a network’s feature maps are divided into channels, and the number of channels, c , can be defined as the width of the layer. A standard CNN layer connects any input channel with any output channel. Hence, the number of convolution kernels per layer is equal to the product of the number of input channels and output channels. Assuming the number of output channels is proportional to the number of input channels, this $\mathcal{O}(c^2)$ growth of operations and parameters causes immense computational challenges. When the number of channels is large, convolutions are the most computationally expensive part of the training and inference of CNNs.

This trend is exacerbated by wide architectures with several hundred or thousand of channels, which are particularly effective in classification tasks involving a large number of classes. Increasing the network’s width is advantageous in terms of accuracy and computational efficiency compared to deeper, narrower networks [62]. However, the quadratic scaling causes the number of weights to reach hundreds of millions and beyond [26], and the computational resources (power and memory) needed for training and running ever-growing CNNs surpasses the resources of common systems [2]. This motivates us to design more efficient network architectures with competitive performance.

1.1. Contribution

We propose a *multigrid-in-channels* (MGIC) approach for building network architectures that enables us to connect all channels at each layer with only $\mathcal{O}(c)$ convolutions

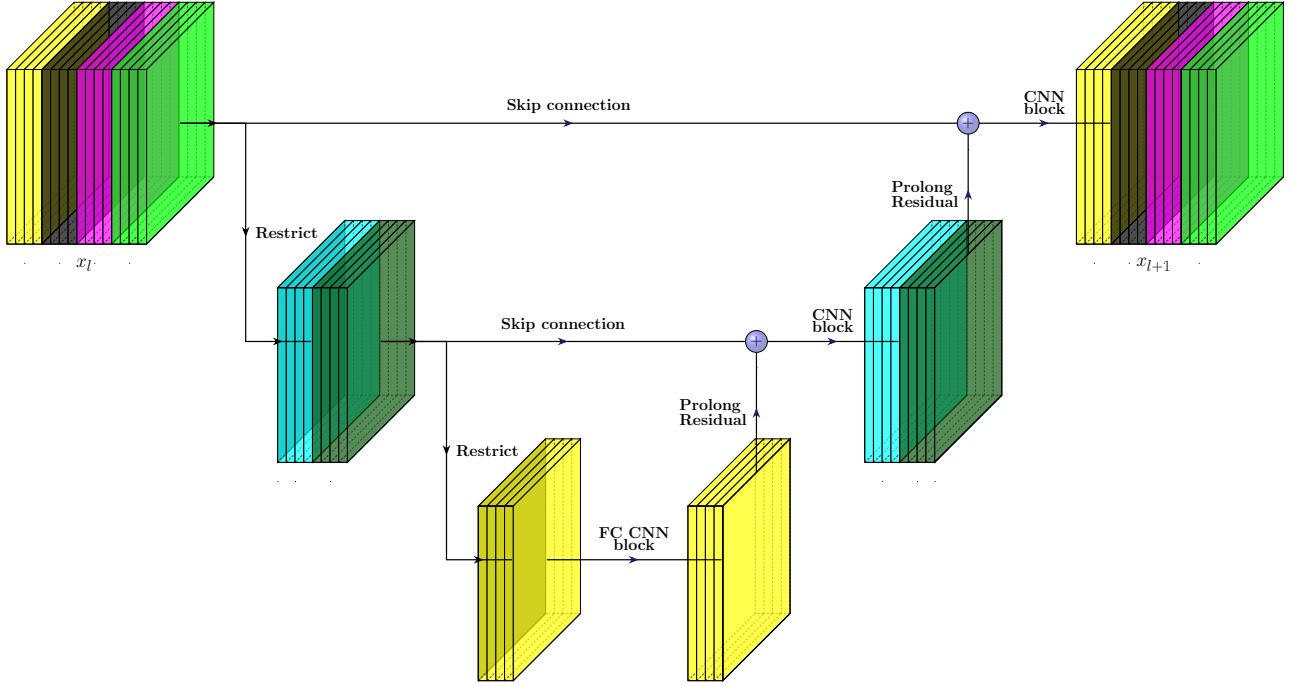


Figure 1: A three-level multigrid block for 16 input channels and a group size of four. *Restrict* and *Prolong Residual* denote grid transfer operators, which decrease and increase the number of channels, respectively. All the channels in the block are of the same spatial resolution. Each color denotes a group of channels that are mixed in a CNN block. The coarsest level uses a fully coupled (FC) CNN block.

and weights. For a given computational budget, this linear scaling allows us to use wider, deeper, and ultimately more expressive networks. Our approach achieves full coupling of the channels via multigrid blocks consisting of grouped convolutions. At each level of the block, a particular width is considered in the channel space. Coarser levels in the block are defined by clusters of channels formed by averaging representative channels from different groups, and therefore have fewer channels. On each level, we apply grouped convolutions on those clustered channels, which effectively connect different fine-level groups. Our MGIC block, which we show in Fig. 1, can replace standard convolutional blocks in CNNs.

Even though our MGIC-block relies on grouped convolutions, its multigrid structure enables the communication between all channels. In our experiments on image classification, segmentation, and point cloud classification tasks, the MGIC-block achieves competitive or superior performance with a relatively low number of parameters and FLOPs.

1.2. Motivation

Multigrid methods [50] are primarily used to solve differential equations and other graphical problems related to diffusion processes (e.g., Markov chains, [43, 48]). Gener-

ally, multigrid methods utilize a hierarchy of grids. They are based on a principle that a local process on a fine grid can only effectively “smooth” the error in an iterative solution process but cannot effectively reduce errors that involve long-distances on the grid. Such errors can be approximated by a suitable procedure on a coarser grid, leading to two advantages. First, coarse grid procedures are less expensive than fine grid procedures as they involve fewer grid points. Second, traversing different scales leads to faster convergence. An alternative interpretation of this paradigm is that the multigrid hierarchy efficiently transfers information across all the grid points using local processing only, at a different scale at each level. Classical multigrid methods rely on the multiscale representation of functions in space but can also be used to tackle temporal problems [13].

In this work, we harness the multigrid approach to obtain full connectivity in networks using locally grouped convolutions. This way, we prevent the redundancy in the number of parameters in CNNs and keep the number of operations and parameters linearly proportional to the network’s width.

2. Related work

Multigrid methods in deep learning. Multigrid has been abundantly applied across the computational sciences, e.g., in partial differential equations [43, 48] and sparse optimization [49, 47] to name a few. Multigrid approaches have also been used to warm-start the training of CNNs on high-resolution images with training on low-resolution images [16], adopting a multiscale approach in space. Similarly, [41, 28] define multiscale architectures that extract and combine features from different resolution images scales. The DeepLabV3 architecture for semantic segmentation [7] also exploits multiscale representations. Other works [6, 9, 51] present different strategies to exploit the spatial multiscale structure and representation of the feature maps throughout CNNs to improve the performance of classical networks. Multigrid has also been used in the layer dimension for residual networks, e.g., to warm-starting the training of a deep network by interpolating the weights of a trained shallow network with a larger step size [4] and parallelizing the training through the layers [15]. While the works mentioned above apply the multigrid idea either in space or in layers (depth), in this work, we use the multigrid idea in the channel space (width).

2.1. Pruning and sparsity

Reducing the number of parameters in CNNs by limiting the connectivity between channels has been a central theme recently. Among the first approaches are the methods of pruning [20, 19, 32] and sparsity [5, 18] that have been typically applied to already trained networks. It has been shown that once a network is trained, a substantial number of its weights can be removed with hardly any degradation of its accuracy. However, the resulting connectivity of these processes may typically be unstructured, which may lead to inefficient deployment of the networks on hardware. While pruning does not save computations during training, it still serves as a proof-of-concept that the full connectivity between channels is superfluous, i.e., there is a redundancy in CNNs [39]. By contrast, we reduce the network architecture by using structured convolution operators, to enable efficient, balanced computations both during training and inference.

2.2. Depth-wise and shuffle convolutions

Another recent effort to reduce the number of parameters of CNNs is to define architectures based on separable convolutions [25, 42, 52, 46, 12, 17, 24]. These CNNs use spatial depth-wise convolution, which filter each input channel separately, and point-wise 1×1 convolutions, which couple all the channels. A popular architecture is MobileNet [25], which involves significantly fewer parameters than standard networks, while achieving comparable performance. The majority of the weights in MobileNets [25, 42, 24] are in the point-wise operators, which scale with $\mathcal{O}(c^2)$. The strength

of MobileNets, and its improvement EfficientNet [46], is the inverse bottleneck structure, that takes a narrow network (with relatively few channels) and expands it by a significant factor to perform the depth-wise and non-linear activation. This way, although the number of parameters scales quadratically in the width in the 1×1 operators, it aims to maximize the spatial convolutions and activations as much as possible to increase the expressiveness of the network. The ShuffleNet [63, 37] reduces the parameters of the point-wise operator by applying 1×1 convolutions to half of the channels and then shuffling them. What sets our approach apart from these efforts is its linear growth of the number of parameters and FLOPs, which enables us to train very wide networks at reduced costs; see Sec. 4.4.

3. Towards efficient convolutions

Typical CNN architectures are composed of a series of blocks

$$\mathbf{x}_{l+1} = \text{CNN-block}(\mathbf{x}_l), \quad (1)$$

where \mathbf{x}_l and \mathbf{x}_{l+1} are the input and output features of the l -th block, respectively. Each CNN-block usually contains a sequence of basic layers, with associated weights which are omitted in the following. To give one common example, consider the bottleneck ResNet block [21] that leads to

$$\mathbf{x}_{l+1} = \mathbf{x}_l + K_{l_3} \sigma(\mathcal{N}(K_{l_2}(\sigma(\mathcal{N}(K_{l_1} \sigma(\mathcal{N}(\mathbf{x}_l)))))). \quad (2)$$

The operators K_{l_1} and K_{l_3} are fully coupled 1×1 convolutions, and K_{l_2} is a 3×3 convolution. σ is a non-linear point-wise activation function, typically the ReLU function $\sigma(x) = \max(x, 0)$. \mathcal{N} is a normalization operator often chosen to be a batch normalization. Architectures that follow a similar trend are MobileNets [25, 42, 24] and ResNeXt [58], in which K_{l_2} is a grouped (or depth-wise) convolution to reduce the number of parameters and increase the ratio between activations and parameters.

A convolution layer takes c_{in} channels of feature maps, and outputs c_{out} such channels. By definition, a fully coupled convolution layer consists of $\mathcal{O}(c_{\text{in}} \cdot c_{\text{out}})$ parameters, and the FLOPs count involved in such convolution also scales quadratically with the width. Since practical implementations of CNNs often use hundreds or thousands of channels, their full coupling leads to large computational costs and to millions of parameters for each layer, which may not be necessary.

To ease the computational costs, all or some of the convolution layers in the CNN block (1) may be grouped, dividing the input channels to several equally-sized groups and applying a separate convolution kernel on each of them. In this work, we denote the number of channels in a group (its size) by s_g . For example, a standard fully-coupled convolution with one group is defined by $s_g = c_{\text{in}}$ where c_{in} is

the number of input channels, while a depth-wise convolution is achieved by $s_g = 1$. As the group size gets smaller, the grouped convolutions involve less computations, at the cost of typically less expressive network architectures. That is because information cannot be shared between different groups in the feature maps during the grouped convolutions.

In this work we propose to replace the CNN-block in (1) by a novel multigrid block to obtain the forward propagation

$$\mathbf{x}_{l+1} = \text{MGIC-block}(\mathbf{x}_l, \text{CNN-block}, s_g, s_c), \quad (3)$$

which, as illustrated in Fig. 1, uses a hierarchy of grids in the channel space and applies the original CNN-block on the coarsest level. The parameter s_g defines the group size of the convolution operators in these CNN-blocks, and s_c is the size of the coarsest grid. As we show in Sec. 4.4, the number of parameters and FLOPs in the MGIC-block scale *linearly* with respect to the number of channels when the group size is fixed.

4. Multigrid-in-channels CNN architectures

In this section, we describe the MGIC-block in detail. We start by defining the multigrid hierarchy. Then, we define the MGIC-block and the grid transfer operators, which are essential to perform down and upsampling of the channel space, followed by a comprehensive description of the design of such MGIC-block. Finally, we compare the computational of a standard CNN layer with ours.

4.1. Multigrid hierarchy

The key idea of our multigrid architecture is to design a hierarchy of grids in the channel space (also referred to as “levels”), where the number of channels in the finest level corresponds to the original width of the network. The number of channels is halved between the levels until reaching the coarsest level, where the number of channels is smaller or equal to the parameter s_c . Our multigrid architecture is accompanied by a CNN block, like the ResNet block in Eq. (2), which is applied on each level. On the finest and intermediate levels, we only connect disjoint groups of channels using grouped convolutions. These convolutions have $\mathcal{O}(c_{\text{in}})$ parameters, as we keep the group size fixed throughout the network, and as the network widens, the number of groups grows. We allow interactions between all the channels on the coarsest grid, where we use the original CNN-block without additional grouping. Since the coarsest grid contains only a few channels, this is not a costly operation.

4.2. The multigrid block

For simplicity, we assume that the CNN-block and the MGIC-block change neither the number of channels nor the spatial resolution of the images. That is, both \mathbf{x}_l and

\mathbf{x}_{l+1} in (3) have c_{in} channels of the same spatial resolution. Given a CNN-block, a group size s_g and coarsest grid size s_c , we define the multigrid block in Algorithm 1, and as an example we present and discuss a two-level version of it below. Here, the two-level hierarchy is denoted by levels 0, 1, and $\mathbf{x}^{(0)} = \mathbf{x}_l$ is the input feature maps on the fine level 0. The two-level block is as follows

$$\mathbf{x}^{(1)} = R_0 \mathbf{x}^{(0)} \quad (4)$$

$$\mathbf{x}^{(1)} \leftarrow \text{CNN-block}(\mathbf{x}^{(1)}) \quad (5)$$

$$\mathbf{x}^{(0)} \leftarrow \mathbf{x}^{(0)} + \mathcal{N}(P_0(\mathbf{x}^{(1)} - R_0 \mathbf{x}^{(0)})) \quad (6)$$

$$\mathbf{x}_{l+1} = \text{CNN-block}(\mathbf{x}^{(0)}, s_g) \quad (7)$$

We first down-sample the channel dimension of the input feature maps $\mathbf{x}^{(0)}$ in Eq. (4) by a factor of 2, using a restriction operator R_0 . This operation creates the coarse feature maps $\mathbf{x}^{(1)}$, which has the same spatial resolution as $\mathbf{x}^{(0)}$, but half the channels. The operator R_0 is implemented by a grouped 1×1 convolution; see also Sec. 4.3. Then, in Eq. (5) a non-grouped CNN block is applied on the coarse feature maps $\mathbf{x}^{(1)}$. This block couples all channels but involves only $c_{\text{in}}^2/4$ parameters instead of c_{in}^2 . Following that, in Eq. (6) we use a prolongation operator P_0 to up-sample the residual $\mathbf{x}^{(1)} - R_0 \mathbf{x}^{(0)}$ from the coarse level to the fine level (up-sampling in channel space) and obtain a feature map with c_{in} channels. Adding the up-sampled residual is common in non-linear multigrid schemes—we elaborate on this point below. Finally, in Eq. (7) we perform a grouped CNN block, which is assumed to be considerably cheaper than a non-grouped version of the CNN block. An illustration of this architecture using three levels is presented in Fig. 1. The multilevel block (Alg. 1) is applied by iteratively reducing the channel space dimensionality until reaching the coarsest grid size s_c .

Since we let the information propagate through the multigrid levels sequentially, we increase the number of convolution layers and non-linear activations compared to the original CNN block. Thereby, we seek to increase the expressiveness of the MGIC-blocks, while limiting their number of weights and computations.

4.3. The choice of transfer operators P_j and R_j

The transfer operators play an important role in multigrid methods. In classical methods, a restriction R maps the fine-level state of the iterative solution onto the coarse grid, and a prolongation P acts in the opposite direction, interpolating the coarse solution back to the fine grid. Clearly, in the coarsening process we lose information, since we reduce the dimension of the problem and the state of the iterate. The key idea is to design P and R such that the coarse problem captures the subspace that is causing the fine-grid process to be inefficient. This results in two complementary processes: the fine-level steps (dubbed as *relaxations* in multigrid literature), and the coarse grid correction.

Algorithm 1: Multigrid-in-channels block

Algorithm:

$\mathbf{x}_{l+1} = \text{MGIC-block}(\mathbf{x}_l, \text{CNN-block}, s_g, s_c)$.

Inputs:

\mathbf{x}_l - input feature map with c_{in} channels.

s_g : group size. s_c : coarsest grid size.

CNN-block: A reference CNN block, e.g., Eq. (2)

$\mathbf{x}^{(0)} = \mathbf{x}_l$

$n_{\text{levels}} = \left\lfloor \log_2 \left(\frac{c_{\text{in}}}{s_c} \right) \right\rfloor$

Going down the levels, starting from \mathbf{x}_l

for $j = 0 : n_{\text{levels}}$ do

| $\mathbf{x}^{(j+1)} = R_j \mathbf{x}^{(j)}$

end

On the coarsest level we perform a non-grouped CNN-block:

$\mathbf{x}^{(n_{\text{levels}})} \leftarrow \text{CNN-block}(\mathbf{x}^{(n_{\text{levels}})})$

Going up the levels:

for $j = n_{\text{levels}} - 1 : 0$ do

| $\mathbf{x}^{(j)} \leftarrow \mathbf{x}^{(j)} + \mathcal{N}(P_j(\mathbf{x}^{(j+1)} - R_j \mathbf{x}^{(j)}))$

| $\mathbf{x}^{(j)} \leftarrow \text{CNN-block}(\mathbf{x}^{(j)}, \text{group_size} = s_g)$

end

return $\mathbf{x}_{l+1} = \mathbf{x}^{(0)}$.

To keep the computations low, we choose R_j to be a grouped 1×1 convolution that halves the number of channels of its operand. We choose P_j to have the transposed structure of R_j . For R_j and P_j we choose the same number of groups as in the CNN-blocks of level j , e.g., for R_0 it will be $\frac{c_{\text{in}}}{s_g}$ groups. The restriction operators take groups of channels of size s_g and using a 1×1 convolution “summerize” the information to $\frac{s_g}{2}$ channels only. In the same way, the prolongation operators interpolate the coarse channels back to the higher channel dimension using grouped 1×1 convolutions. This choice for the transfer operators corresponds to aggregation-based multigrid coarsening [48], where aggregates (groups) of variables are averaged to form a coarse grid variable. In Sec. 5.1, we exemplify that the transfer operators preserve essential information of all channels.

The weights of the transfer operators (the grouped convolutions) are learned as part of the optimization, and are initialized by positive weights with row-sums of 1. That is, they are initialized to average feature maps within the same group. The purpose of this initialization is that the feature maps will not vanish initially as we multiply them by consecutive restrictions R_j to start the MGIC-block.

The importance of up-sampled residuals. Adding the up-sampled residual in (6) is the standard way to apply multigrid methods to solve non-linear problems [50, 59]. Here, it allows us to have a skip connection between corresponding levels of the multigrid, introducing an identity mapping in

(6) as guided by [21]. To prevent exploding gradients by feature maps summation, at each level j we prolong only a residual defined by subtracting the matching feature maps before and after traversing the levels $j+1, \dots, n_{\text{levels}}$. By this definition, if the CNN-block has an identity mapping, the whole MGIC-block in Alg. 1 also has an identity mapping.

Changing resolution blocks. The structure of the MGIC block as in Fig. 1 is more natural to equal input and output channel sizes, i.e., $c_{\text{in}} = c_{\text{out}}$. Hence, when we wish to change the number of channels (usually following a stride), we define a lightweight shortcut that is designed to bring a tensor from c_{in} to c_{out} such that our MGIC-blocks will be given an input where $c_{\text{in}} = c_{\text{out}}$. Specifically, we use a depth-wise 3×3 convolution.

4.4. The complexity of the MGIC-block

Consider a case where we have $c = c_{\text{in}} = c_{\text{out}}$ channels in the network, and we apply a standard convolution layer using $d \times d$ convolution kernels (e.g., a 3×3 kernel). The output consists of c feature maps, where each one is a sum of the c input maps, each convolved with a kernel. Hence, such a convolution layer requires $\mathcal{O}(c^2 \cdot d^2)$ parameters, inducing a quadratic growth in the parameters and FLOPs.

Now, assume that we apply an MGIC block with one convolution at each level and a group size of s_g . Such a grouped convolution has $c \cdot s_g \cdot d^2$ parameters. Each coarsening step divides c by 2 until the coarsest level is reached, and a fully coupled convolution with $s_c^2 \cdot d^2$ parameters is used. For n levels, the number of parameters is

$$\sum_{j=0}^{n-1} \left(\frac{s_g \cdot c \cdot d^2}{2^j} \right) + s_c^2 \cdot d^2 < 2(s_g \cdot c \cdot d^2) + s_c^2 \cdot d^2. \quad (8)$$

If s_c is small, we can neglect the second term and get $\mathcal{O}(s_g \cdot c \cdot d^2)$ parameters. Therefore, since s_g and s_c are fixed and small, our method scales linearly with respect to the networks’ width. This will be most beneficial if n is large (e.g. in wide stages of networks).

5. Experiments

In this section, we report several experiments with our MGIC approach. We start with a toy experiment, measuring how well it can compress the channel space. Then, we test our method on image classification and segmentation and point cloud classification benchmarks. Our goal is to compare how different architectures perform using a relatively small number of parameters, aiming to achieve similar or better results with fewer parameters and FLOPs. We train all our models using NVIDIA Titan RTX and implement our code using the PyTorch software [40].

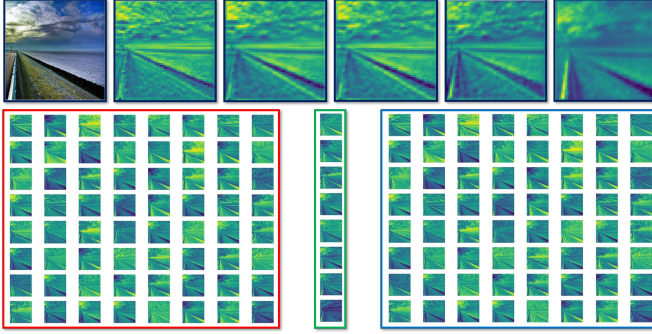


Figure 2: From left to right: Top - input image, one of its feature maps, and its reconstructions with $s_g = 32, 16, 8, 4$, respectively. s_c is kept at 8. Bottom - input feature maps, their coarsest grid representation, and their reconstruction from our MGIC block with down and up-sampling only.

Table 1: Feature maps reconstruction MSE v.s. s_g . s_c is fixed to 8.

s_g	32	16	8	4
MSE (10^{-3})	11	13	17	24
Parameters [K]	3.3	1.8	0.9	0.4

5.1. Coarse channels representation experiment

As we explain in Sec. 4, our method aims to reduce parameters and FLOPs by introducing a hierarchical representation of the channels of the network, and let the forward application of the network traverse all this hierarchy. Therefore, in this experiment we are interested in quantifying the effectiveness of our approach’s channel down and up sampling mechanism. Specifically, we wish to measure how well we can encode feature maps on the coarsest grid. To do so, we sample 1,024 images from ImageNet, and extract their feature maps from the first convolutional layer of a pre-trained ResNet-50. Then, we encode and decode those feature maps using the restriction and prolongation operators, respectively. To study the transfer operators in isolation, we remove the CNN blocks and long skip connections shown in Fig. 1 from the MGIC-block. We experiment with several values of the group size parameter s_g and present the mean squared error of the feature maps reconstruction in Tab. 1. We also show the original feature maps and their reconstructions in Fig. 2. According to this experiment, our method is able to faithfully represent the original channel space, even when it operates on a low parameters and FLOPs budget.

5.2. Image classification

We compare our approach with a variety of popular and recent networks like ResNet-50 [21], MobileNetV3 [24] and GhostNet [17] for image classification on the CIFAR10 and

Table 2: Comparison of state-of-the-art methods for compressing ResNet-56 on CIFAR-10. - represents no reported results available.

Architecture	Params [M]	FLOPs [M]	Test acc.
ResNet-56 [21]	0.85	125	93.0%
CP-ResNet-56 [23]	-	63	92.0%
ℓ_1 -ResNet-56 [33, 35]	0.73	91	92.5%
AMC-ResNet-56 [22]	-	63	91.9%
Ghost-ResNet-56 (s=2) [17]	0.43	63	92.7%
MGIC - ResNet-56 (ours)	0.41	60	94.2%

ImageNet dataset. We use SGD optimizer with a mini-batch size of 256 for ImageNet, and 128 for CIFAR-10, both for 180 epochs. Our loss function is cross-entropy. The initial learning rates for CIFAR-10 and ImageNet are 0.001 and 0.1, respectively. We divide them by 10 every 30 epochs. The weight decay is 0.0001, and the momentum is 0.9. As data augmentation, for both datasets, we use standard random horizontal flipping and crops, as in [21].

5.2.1 CIFAR-10

The CIFAR-10 dataset [29] consists of 60K natural images of size 32×32 with labels assigning each image into one of ten categories. The data is split into 50K training and 10K test sets. Here, we use a ResNet-56 [21] architecture together with our MGIC block, with parameters $s_g = 8, s_c = 16$. We compare our method with other recent and popular architectures such as AMC-ResNet-56 [22] and Ghost-ResNet-56 [17], and our baseline is the original ResNet-56. We report our results in Tab. 2, where we see large improvement over existing methods, while retaining low number of parameters and FLOPs.

5.2.2 ImageNet

The ImageNet [1] challenge ILSVRC 2012 consists of over 1.28M training images and 50K validation images from 1000 categories. We follow [21] and resize the images to a size of 224×224 . We perform two experiments as described below.

ResNet-50 compression. We compress the ResNet-50 architecture (parameter and FLOPs wise), and compare our MGIC approach with other methods. The results are reported in Table 3, where we propose three variants of our MGIC-ResNet-50 network, differing in their parameters s_g and s_c . Our results outperform the rest of the considered methods, and our network with $s_g = 64, s_c = 64$ also obtains better performance than ResNeXt-50 [58] (25.0M parameters, 4.2B FLOPs, 77.8% top-1 accuracy), which is not shown in the table because the ResNeXt architecture

Table 3: Comparison of state-of-the-art methods for compressing ResNet-50 on ImageNet dataset.

Model	Params [M]	FLOPs [B]	Top-1 Acc. %	Top-5 Acc. %
ResNet-50 [21]	25.6	4.1	75.3	92.2
Thinet-ResNet-50 [36]	16.9	2.6	72.1	90.3
NISP-ResNet-50-B [61]	14.4	2.3	-	90.8
Versatile-ResNet-50 [54]	11.0	3.0	74.5	91.8
SSS-ResNet-50 [27]	-	2.8	74.2	91.9
Ghost-ResNet-50 [17]	13.0	2.2	75.0	92.3
MGIC-ResNet-50 ($s_g = 32, s_c = 64$) (ours)	9.4	1.6	75.8	92.9
MGIC-ResNet-50 ($s_g = 64, s_c = 64$) (ours)	15.1	2.5	77.9	93.7
Shift-ResNet-50 [56]	6.0	-	70.6	90.1
Taylor-FO-BN-ResNet-50 [38]	7.9	1.3	71.7	-
Slimmable-ResNet-50 0.5x [60]	6.9	1.1	72.1	-
MetaPruning-ResNet-50 [34]	-	1.0	73.4	-
Ghost-ResNet-50 (s=4) [17]	6.5	1.2	74.1	91.9
MGIC-ResNet-50 ($s_g = 16, s_c = 64$) (ours)	6.2	1.0	74.3	92.0

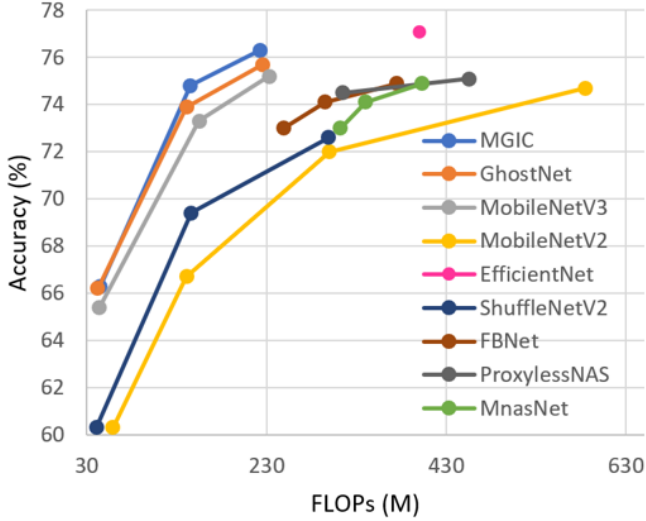


Figure 3: Top-1 accuracy v.s. FLOPs on ImageNet dataset.

utilizes more channels than ResNet-50 and therefore is not directly comparable.

ImageNet classification on a budget of FLOPs. The second experiment compares our approach with recent light networks like ShuffleNets [37, 64], MobileNets [25, 42, 24] and GhostNet [17]. We follow the MobileNetV3-Large [24] architecture for its efficiency and high accuracy, and replace the standard MobileNetV3 block with our MGIC block, configured to $s_g = 64, s_c = 64$. Our experiment is divided to three scales - small, medium and large, where we scale our networks with width factors of 0.6, 1.0 and 1.2, respectively.

We find that our method obtains higher accuracy, with similar number of FLOPs. We present our results in Table 4 and Fig. 3.

5.3. Image segmentation

We compare our method with MobileNetV3 on semantic segmentation on the Cityscapes [10] dataset. For the encoder part of the network, we build large and small variants, based on MobileNetV3-Large and MobileNetV3-Small, which are described in Tables 1-2 in [24], respectively. We also utilize the proposed LR-ASPP segmentation head, and follow the observations from [24]. Namely, we reduce the number of channels in the last block of our networks by a factor of two and use 128 filters in the segmentation head. For training, we use the same data augmentation and optimization approach as in [7]. The results are shown in Tab. 5.

5.4. Point cloud classification

The experiments in previous sections were performed on structured CNNs, i.e., on 2D images. To further validate the generalization and usefulness of our method, we incorporate it in graph convolutional networks (GCNs) to perform point cloud classification. Specifically, we use a smaller version of the architecture from [53], where we alter the width of the last three classifier layers from 1024, 512, 256 to 64 in all of them. In all networks we define the adjacency matrix using k-NN algorithm with $k = 10$. Then, we replace the GCN block with each of the backbones listed in Tab. 6, where we also report their performance on point-cloud classification on ModelNet-10 [57] benchmark where we sample 1,024 points from each shape.

Table 4: Comparison of state-of-the-art small networks on ImageNet dataset classification.

Model	Params [M]	FLOPs [M]	Top-1 Acc. %	Top-5 Acc. %
ShuffleNetV1 0.5x (g=8) [64]	1.0	40	58.8	81.0
MobileNetV2 0.35x [42]	1.7	59	60.3	82.9
ShuffleNetV2 0.5x [37]	1.4	41	61.1	82.6
MobileNetV3-Small 0.75x [24]	2.4	44	65.4	-
GhostNet 0.5x [17]	2.6	42	66.2	86.6
MGIC-MobileNetV3 0.6x (ours)	2.3	48	66.3	86.8
MobileNetV1 0.5x [25]	1.3	150	63.3	84.9
MobileNetV2 0.6x [42]	2.2	141	66.7	-
ShuffleNetV1 1.0x (g=3) [64]	1.9	138	67.8	87.7
ShuffleNetV2 1.0x [37]	2.3	146	69.4	88.9
MobileNetV3-Large 0.75x [24]	4.0	155	73.3	-
GhostNet 1.0x [17]	5.2	141	73.9	91.4
MGIC-MobileNetV3 1.0x (ours)	5.2	145	74.8	92.0
MobileNetV2 1.0x [42]	3.5	300	71.8	91.0
ShuffleNetV2 1.5x [37]	3.5	299	72.6	90.6
FE-Net 1.0x [8]	3.7	301	72.9	-
FBNet-B [55]	4.5	295	74.1	-
ProxylessNAS [3]	4.1	320	74.6	92.2
MnasNet-A1 [45]	3.9	312	75.2	92.5
MobileNetV3-Large [24] 1.0x	5.4	219	75.2	-
GhostNet 1.3x [17]	7.3	226	75.7	92.7
MGIC-MobileNetV3 1.2x (ours)	7.1	233	76.1	93.2

Table 5: Segmentation results on Cityscapes dataset. Metric is in mean intersection over union.

Backbone	Params[M]	FLOPs [B]	mIoU %
MobileNetV3-Large [24]	1.51	9.74	72.64
MobileNetV3-Small [24]	0.47	2.90	68.38
MGIC-Large (ours)	1.67	9.62	72.60
MGIC-Small (ours)	0.48	2.73	68.52

Table 6: ModelNet-10 classification.

Backbone	Params[M]	FLOPs [M]	Accuracy %
DGCNN [53]	0.16	125	91.6
diffGCN [11]	0.57	64	92.5
MGIC-diffGCN (ours)	0.11	13.7	92.9

5.5. Ablation study

In order to determine the impact of the our block parameters s_g and s_c , we perform two experiments on CIFAR-10 for image classification. First, we fix s_g to 16, and observe how the number of parameters, FLOPs and accuracy of our MGIC-ResNet-56 change. In the second experiment, we fix

Table 7: Influence of s_c in our MGIC framework on ResNet-56 architecture and CIFAR-10 dataset. s_g is fixed to 16.

s_c	Params[M]	FLOPs [M]	Accuracy %
64	0.53	91	94.7
32	0.5	76	94.6
16	0.47	65	94.3

Table 8: Influence of s_g in our MGIC framework on ResNet-56 architecture and CIFAR-10 dataset. s_c is fixed to 16.

s_g	Params[M]	FLOPs [M]	Accuracy %
32	0.79	100	94.8
16	0.53	85	94.7
8	0.41	60	94.2
4	0.29	45	92.8

s_c to 16, while modifying s_g , we examine the behavior of our model. The results are reported in Tables 7-8.

6. Conclusion

We present a novel multigrid-in-channels (MGIC) approach that improves the efficiency of convolutional neural networks (CNN) both in parameters and FLOPs, while using easy to implement structured grouped convolutions in the channel space. Applying MGIC, we achieve full coupling through a multilevel hierarchy of the channels, at only $\mathcal{O}(c)$ cost, unlike standard convolution layers that require $\mathcal{O}(c^2)$. MGIC is most beneficial for wide networks. Our experiments for various tasks suggest that MGIC achieves comparable or superior accuracy than other recent light-weight architectures at a given budget. Our MGIC block offers a universal approach for producing light-weight versions of networks suitable for different kinds of CNNs, GCNs, and traditional NNs, where fully-connected layers are applied.

Acknowledgement

This research was partially supported by grant no. 2018209 from the United States - Israel Binational Science Foundation (BSF), Jerusalem, Israel. ME is supported by Kreitman High-tech scholarship.

References

- [1] <http://www.image-net.org/>, 2020. [Online; accessed May-2019].
- [2] Monica Bianchini and Franco Scarselli. On the complexity of neural network classifiers: A comparison between shallow and deep architectures. *IEEE transactions on neural networks and learning systems*, 25(8):1553–1565, 2014.
- [3] Han Cai, Ligeng Zhu, and Song Han. Proxylessnas: Direct neural architecture search on target task and hardware. *arXiv preprint arXiv:1812.00332*, 2018.
- [4] Bo Chang, Lili Meng, Eldad Haber, Frederick Tung, and David Begert. Multi-level residual networks from dynamical systems view. *arXiv preprint arXiv:1710.10348*, 2017.
- [5] Soravit Changpinyo, Mark Sandler, and Andrey Zhmoginov. The power of sparsity in convolutional neural networks, 2017.
- [6] Chun-Fu Chen, Quanfu Fan, Neil Mallinar, Tom Sercu, and Rogerio Feris. Big-little net: An efficient multi-scale feature representation for visual and speech recognition. 2019.
- [7] Liang-Chieh Chen, George Papandreou, Florian Schroff, and Hartwig Adam. Rethinking atrous convolution for semantic image segmentation. *arXiv preprint arXiv:1706.05587*, 2017.
- [8] Weijie Chen, Di Xie, Yuan Zhang, and Shiliang Pu. All you need is a few shifts: Designing efficient convolutional neural networks for image classification. In *Proceedings of the IEEE Conference on Computer Vision and Pattern Recognition*, pages 7241–7250, 2019.
- [9] Yunpeng Chen, Haoqi Fan, Bing Xu, Zhicheng Yan, Yannis Kalantidis, Marcus Rohrbach, Shuicheng Yan, and Jiashi Feng. Drop an Octave: Reducing spatial redundancy in convolutional neural networks with octave convolution. In *Proceedings of the IEEE International Conference on Computer Vision (ICCV)*, pages 3435–3444, 2019.
- [10] Marius Cordts, Mohamed Omran, Sebastian Ramos, Timo Rehfeld, Markus Enzweiler, Rodrigo Benenson, Uwe Franke, Stefan Roth, and Bernt Schiele. The cityscapes dataset for semantic urban scene understanding. In *Proc. of the IEEE Conference on Computer Vision and Pattern Recognition (CVPR)*, 2016.
- [11] Moshe Eliasof and Eran Treister. Diffgcn: Graph convolutional networks via differential operators and algebraic multigrid pooling, 2020.
- [12] Jonathan Ephrath, Moshe Eliasof, Lars Ruthotto, Eldad Haber, and Eran Treister. Leancnnets: Low-cost yet effective convolutional neural networks. *IEEE Journal of Selected Topics in Signal Processing*, 2020.
- [13] Robert D Falgout, Stephanie Friedhoff, Tz V Kolev, Scott P MacLachlan, and Jacob B Schroder. Parallel time integration with multigrid. *SIAM Journal on Scientific Computing*, 36(6):C635–C661, 2014.
- [14] Ross Girshick, Jeff Donahue, Trevor Darrell, and Jitendra Malik. Rich feature hierarchies for accurate object detection and semantic segmentation. In *Proceedings of the IEEE conference on computer vision and pattern recognition*, pages 580–587, 2014.
- [15] Stefanie Gunther, Lars Ruthotto, Jacob B Schroder, Eric C Cyr, and Nicolas R Gauger. Layer-parallel training of deep residual neural networks. *SIAM Journal on Mathematics of Data Science*, 2(1):1–23, 2020.
- [16] Eldad Haber, Lars Ruthotto, Elliot Holtham, and Seong-Hwan Jun. Learning across scales—multiscale methods for convolution neural networks. In *Thirty-Second AAAI Conference on Artificial Intelligence*, 2018.
- [17] Kai Han, Yunhe Wang, Qi Tian, Jianyuan Guo, Chunjing Xu, and Chang Xu. Ghostnet: More features from cheap operations. In *Proceedings of the IEEE/CVF Conference on Computer Vision and Pattern Recognition*, pages 1580–1589, 2020.
- [18] Song Han, Jeff Pool, Sharan Narang, Huizi Mao, Enhao Gong, Shijian Tang, Erich Elsen, Peter Vajda, Manohar Paluri, John Tran, Bryan Catanzaro, and William J. Dally. DSD: Dense-sparse-dense training for deep neural networks. In *Proceedings of the International Conference on Learning Representations (ICLR)*, 2017.
- [19] Song Han, Jeff Pool, John Tran, and William J. Dally. Learning both weights and connections for efficient neural network. *International Journal of Computer Vision*, 5(5):1135–1143, 2015.
- [20] Babak Hassibi and David G. Stork. Second order derivatives for network pruning: Optimal brain surgeon reconstruction. *International Journal of Computer Vision*, 5(5):164–171, 1992.
- [21] Kaiming He, Xiangyu Zhang, Shaoqing Ren, and Jian Sun. Deep residual learning for image recognition. In *Proceedings of the IEEE Conference on Computer Vision and Pattern Recognition*, pages 770–778, 2016.
- [22] Yihui He, Ji Lin, Zhijian Liu, Hanrui Wang, Li-Jia Li, and Song Han. Amc: Automl for model compression and acceleration on mobile devices. In *Proceedings of the European Conference on Computer Vision (ECCV)*, pages 784–800, 2018.

[23] Yihui He, Xiangyu Zhang, and Jian Sun. Channel pruning for accelerating very deep neural networks. In *Proceedings of the IEEE International Conference on Computer Vision*, pages 1389–1397, 2017.

[24] Andrew Howard, Mark Sandler, Grace Chu, Liang-Chieh Chen, Bo Chen, Mingxing Tan, Weijun Wang, Yukun Zhu, Ruoming Pang, Vijay Vasudevan, et al. Searching for mobilenetv3. In *Proceedings of the IEEE International Conference on Computer Vision*, pages 1314–1324, 2019.

[25] Andrew G Howard, Menglong Zhu, Bo Chen, Dmitry Kalenichenko, Weijun Wang, Tobias Weyand, Marco Andreetto, and Hartwig Adam. MobileNets: Efficient convolutional neural networks for mobile vision applications. *arXiv preprint arXiv:1704.04861*, 2017.

[26] Yanping Huang, Youlong Cheng, Ankur Bapna, Orhan Firat, Dehao Chen, Mia Chen, HyoukJoong Lee, Jiquan Ngiam, Quoc V Le, Yonghui Wu, et al. Gpipe: Efficient training of giant neural networks using pipeline parallelism. In *Advances in Neural Information Processing Systems*, pages 103–112, 2019.

[27] Zehao Huang and Naiyan Wang. Data-driven sparse structure selection for deep neural networks. In *Proceedings of the European conference on computer vision (ECCV)*, pages 304–320, 2018.

[28] Tsung-Wei Ke, Michael Maire, and Stella X. Yu. Multigrid neural architectures. <https://arxiv.org/abs/1611.07661>, 2017.

[29] Alex Krizhevsky and Geoffrey Hinton. Learning multiple layers of features from tiny images. 2009.

[30] Alex Krizhevsky, Ilya Sutskever, and Geoffrey E Hinton. Imagenet classification with deep convolutional neural networks. In *Advances in neural information processing systems*, pages 1097–1105, 2012.

[31] Y LeCun, B E Boser, and J S Denker. Handwritten digit recognition with a back-propagation network. In *Advances in neural information processing systems*, pages 396–404, 1990.

[32] Hao Li, Asim Kadav, Igor Durdanovic, Hanan Samet, and Hans Peter Graf. Pruning filters for efficient ConvNets. In *Proceedings of the International Conference on Learning Representations (ICLR)*, 2017.

[33] Hao Li, Asim Kadav, Igor Durdanovic, Hanan Samet, and Hans Peter Graf. Pruning filters for efficient convnets, 2017.

[34] Zechun Liu, Haoyuan Mu, Xiangyu Zhang, Zichao Guo, Xin Yang, Kwang-Ting Cheng, and Jian Sun. Metapruning: Meta learning for automatic neural network channel pruning. In *Proceedings of the IEEE International Conference on Computer Vision*, pages 3296–3305, 2019.

[35] Zhuang Liu, Mingjie Sun, Tinghui Zhou, Gao Huang, and Trevor Darrell. Rethinking the value of network pruning. *arXiv preprint arXiv:1810.05270*, 2018.

[36] Jian-Hao Luo, Jianxin Wu, and Weiyao Lin. Thinet: A filter level pruning method for deep neural network compression. In *Proceedings of the IEEE international conference on computer vision*, pages 5058–5066, 2017.

[37] Ningning Ma, Xiangyu Zhang, Hai-Tao Zheng, and Jian Sun. ShuffleNet V2: Practical guidelines for efficient CNN architecture design. In *Proceedings of the European Conference on Computer Vision (ECCV)*, pages 116–131, 2018.

[38] Pavlo Molchanov, Arun Mallya, Stephen Tyree, Iuri Frosio, and Jan Kautz. Importance estimation for neural network pruning. In *Proceedings of the IEEE Conference on Computer Vision and Pattern Recognition*, pages 11264–11272, 2019.

[39] Pavlo Molchanov, Stephen Tyree, Tero Karras, Timo Aila, and Jan Kautz. Pruning convolutional neural networks for resource efficient transfer learning. In *Proceedings of the International Conference on Learning Representations (ICLR)*, 2017.

[40] Adam Paszke, Sam Gross, Soumith Chintala, Gregory Chanan, Edward Yang, Zachary DeVito, Zeming Lin, Alban Desmaison, Luca Antiga, and Adam Lerer. Automatic differentiation in pytorch. In *Advances in Neural Information Processing Systems*, 2017.

[41] Daniël M Pelt and James A Sethian. A mixed-scale dense convolutional neural network for image analysis. *Proceedings of the National Academy of Sciences*, 115(2):254–259, 2018.

[42] Mark Sandler, Andrew Howard, Menglong Zhu, Andrey Zhmoginov, and Liang-Chieh Chen. MobileNetV2: Inverted residuals and linear bottlenecks. In *Proceedings of the IEEE Conference on Computer Vision and Pattern Recognition*, pages 4510–4520, 2018.

[43] Hans De Sterck, Killian Miller, Eran Treister, and Irad Yavneh. Fast multilevel methods for markov chains. *Numerical Linear Algebra with Applications*, 18(6):961–980, 2011.

[44] Christian Szegedy, Wei Liu, Yangqing Jia, Pierre Sermanet, Scott Reed, Dragomir Anguelov, Dumitru Erhan, Vincent Vanhoucke, and Andrew Rabinovich. Going deeper with convolutions. In *Proceedings of the IEEE conference on computer vision and pattern recognition*, pages 1–9, 2015.

[45] Mingxing Tan, Bo Chen, Ruoming Pang, Vijay Vasudevan, Mark Sandler, Andrew Howard, and Quoc V Le. Mnasnet: Platform-aware neural architecture search for mobile. In *Proceedings of the IEEE Conference on Computer Vision and Pattern Recognition*, pages 2820–2828, 2019.

[46] Mingxing Tan and Quoc V Le. Efficientnet: Rethinking model scaling for convolutional neural networks. In *International Conference on Machine Learning (ICML)*, 2019.

[47] Eran Treister, Javier S Turek, and Irad Yavneh. A multilevel framework for sparse optimization with application to inverse covariance estimation and logistic regression. *SIAM Journal on Scientific Computing*, 38(5):S566–S592, 2016.

[48] Eran Treister and Irad Yavneh. On-the-fly adaptive smoothed aggregation multigrid for markov chains. *SIAM Journal on Scientific Computing*, 33(5):2927–2949, 2011.

[49] Eran Treister and Irad Yavneh. A multilevel iterated-shrinkage approach to l_1 penalized least-squares minimization. *IEEE Transactions on Signal Processing*, 60(12):6319–6329, 2012.

[50] Ulrich Trottenberg, Cornelius W Oosterlee, and Anton Schuller. *Multigrid*. Elsevier, 2000.

[51] Huiyu Wang, Aniruddha Kembhavi, Ali Farhadi, Alan L Yuille, and Mohammad Rastegari. Elastic: Improving cnns with dynamic scaling policies. In *Proceedings of the IEEE Conference on Computer Vision and Pattern Recognition (CVPR)*, pages 2258–2267, 2019.

[52] Min Wang, Baoyuan Liu, and Hassan Foroosh. Design of efficient convolutional layers using single intra-channel con-

volution, topological subdivisioning and spatial "bottleneck" structure, 2016.

[53] Yue Wang, Yongbin Sun, Ziwei Liu, Sanjay E. Sarma, Michael M. Bronstein, and Justin M. Solomon. Dynamic graph cnn for learning on point clouds. *ACM Transactions on Graphics (TOG)*, 2019.

[54] Yunhe Wang, Chang Xu, XU Chunjing, Chao Xu, and Dacheng Tao. Learning versatile filters for efficient convolutional neural networks. In *Advances in Neural Information Processing Systems*, pages 1608–1618, 2018.

[55] Bichen Wu, Xiaoliang Dai, Peizhao Zhang, Yanghan Wang, Fei Sun, Yiming Wu, Yuandong Tian, Peter Vajda, Yangqing Jia, and Kurt Keutzer. Fbnet: Hardware-aware efficient convnet design via differentiable neural architecture search. In *Proceedings of the IEEE Conference on Computer Vision and Pattern Recognition*, pages 10734–10742, 2019.

[56] Bichen Wu, Alvin Wan, Xiangyu Yue, Peter Jin, Sicheng Zhao, Noah Golmant, Amir Gholaminejad, Joseph Gonzalez, and Kurt Keutzer. Shift: A zero flop, zero parameter alternative to spatial convolutions. In *Proceedings of the IEEE Conference on Computer Vision and Pattern Recognition*, pages 9127–9135, 2018.

[57] Zhirong Wu, Shuran Song, Aditya Khosla, Fisher Yu, Lin-guang Zhang, Xiaoou Tang, and Jianxiong Xiao. 3d shapenets: A deep representation for volumetric shapes. In *Proceedings of the IEEE conference on computer vision and pattern recognition*, pages 1912–1920, 2015.

[58] Saining Xie, Ross Girshick, Piotr Dollár, Zhuowen Tu, and Kaiming He. Aggregated residual transformations for deep neural networks. In *Proceedings of the IEEE conference on computer vision and pattern recognition*, pages 1492–1500, 2017.

[59] Irad Yavneh and Gregory Dardyk. A multilevel nonlinear method. *SIAM journal on scientific computing*, 28(1):24–46, 2006.

[60] Jiahui Yu, Linjie Yang, Ning Xu, Jianchao Yang, and Thomas Huang. Slimmable neural networks. *arXiv preprint arXiv:1812.08928*, 2018.

[61] Ruichi Yu, Ang Li, Chun-Fu Chen, Jui-Hsin Lai, Vlad I Morariu, Xintong Han, Mingfei Gao, Ching-Yung Lin, and Larry S Davis. Nisp: Pruning networks using neuron importance score propagation. In *Proceedings of the IEEE Conference on Computer Vision and Pattern Recognition*, pages 9194–9203, 2018.

[62] Sergey Zagoruyko and Nikos Komodakis. Wide residual networks. In Edwin R. Hancock Richard C. Wilson and William A. P. Smith, editors, *Proceedings of the British Machine Vision Conference (BMVC)*, pages 87.1–87.12. BMVA Press, September 2016.

[63] Xiangyu Zhang, Xinyu Zhou, Mengxiao Lin, and Jian Sun. ShuffleNet: An extremely efficient convolutional neural network for mobile devices. In *Proceedings of the IEEE Conference on Computer Vision and Pattern Recognition*, pages 6848–6856, 2018.

[64] Xiangyu Zhang, Xinyu Zhou, Mengxiao Lin, and Jian Sun. Shufflenet: An extremely efficient convolutional neural network for mobile devices. In *Proceedings of the IEEE conference on computer vision and pattern recognition*, pages 6848–6856, 2018.